Structure Sensitivity of 2-methyl-3-butyn-2-ol Hydrogenation on Pd: Computational and Experimental Modeling

Antonio Prestianni,[†] Micaela Crespo-Quesada,[‡] Remedios Cortese,[†] Francesco Ferrante,[†] Liubov Kiwi-Minsker,[‡] and Dario Duca*[,†]

Dipartimento di Fisica e Chimica, Università degli Studi di Palermo, viale delle Scienze Ed. 17, I-90128 Palermo, and Group of Catalytic Reaction Engineering, Ecole Polytechnique Fédérale de Lausanne, CH-1015 Lausanne

E-mail: dduca@cccp.unipa.it

Phone: +39(091)238-97975. Fax: +39(091)590015

Abstract

In the frame of DFT paradigms, the adsorption of 2-methyl-3-butyn-2-ol (MBY) and 2-methyl-3-buten-2-ol (MBE) on a Pd_{30} cluster, including both {100} and {111} faces, was studied along with the pathways involved in the hydrogenation, taking place on plane and low coordination (corner/edge) sites of given MBY/Pd_{30} and MBE/Pd_{30} surface configurations. The calculated energetics – further validated by gas-phase and water-assisted-gas-phase MBY and MBE hydrogenation, performed on well-defined size and shape-controlled Pd nanoparticles supported on SiO_2 – were able to explain the origin of the structure sensitivity and the high selectivity characterizing the title reaction when occurring in aqueous solution. The C≡C

*To whom correspondence should be addressed

[†]Dipartimento di Fisica e Chimica, Università degli Studi di Palermo, viale delle Scienze Ed. 17, I-90128 Palermo

[‡]Group of Catalytic Reaction Engineering, Ecole Polytechnique Fédérale de Lausanne, CH-1015 Lausanne

moiety of the MBY surface species indeed seemed to be mostly activated by plane sites instead of corner/edge atoms whereas the MBE species appeared to have a different behavior, being their C=C moieties typically activated by low coordination sites. DFT studies excluded that the over-hydrogenation paths could be affected by the site topologies hence the role of plane, edge or corner atoms should not be influential in setting the surface reaction mechanism, which as a consequence could be controlled by the adsorption energy, actually, distinguished by different values on sites of different topology. The role of water in the selectivity to MBE, which characterizes the catalytic over-hydrogenation of MBY on Pd nanoparticles, was also inferred.

Keywords: Structure sensitivity, unsaturated alchool hydrogenation, palladium nanoparticle catalyst

Introduction

The catalytic hydrogenation of alkynes is a key process in the fine and intermediate chemical industry.[1,2] Amongst the wide variety of metals capable of fully saturating alkynes under mild conditions, Pd is considered to be the most performing in terms of alkene yield.[2] The morphology (shape and size) of the active metal nanoparticles has a great impact on their catalytic performance.[3] These two structural descriptors were firstly linked to the catalytic activity in the seminal investigations performed by Boudart, who classified catalytic reactions into either structure sensitive or insensitive, depending on the observed influence of the metal crystallite size and shape (hence, of the topological properties of the different metallic planes involved) on the catalytic activity, namely on the turnover frequency (TOF).[4,5]

The first study concerning nanoparticle size effects[6] was published in 1983 by Boitiaux et al. However, the catalysts usually employed in such studies were prepared using different stabilizing agents and conditions, which ruled not only the metal crystallite size but other important chemical and structural properties of the catalyst, able to affect the catalytic performances. Thus, the early

results concerning size effects on the alkyne selective hydrogenation are, up to now, rather controversial,[7] although some consensus emerges pointing towards higher activity for larger particles, *i.e.* TOF decreases along with the metal dispersion.[8–12]

In terms of nanoparticle shape effects, there is a limited number of work available in the open literature, particularly for alkyne hydrogenation.[13,14] The advances in colloidal preparation of metal nanostructures provide catalytic metal particles with size and/or shape variation without other alterations,[15,16] thus rendering them excellent materials suitable for catalytic investigations. For example, Telkar et al. demonstrated a relationship between shape and TOF for cubic and spherical nanoparticles in the hydrogenation of 2-butyne-1,4-diol.[17] Yarulin et al. also showed that {111} planes were more active than the {100} ones in the hydrogenation of acetylene over shape-controlled C-supported Pd cubes and cube-octahedra.[18] In this line, we have recently found that the hydrogenation in aqueous medium of 2-methyl-3-butyn-2-ol (MBY) occurring on Pd nanocrystals, having well-defined shapes, is a structure sensitive reaction. In particular, the semi-hydrogenation of MBY to 2-methyl-3-buten-2-ol (MBE) occurred preferentially on the plane sites irrespective of their crystallographic orientation, namely {111} and/or {100} planes, whereas the over-hydrogenation to 2-methyl-3-butan-2-ol (MBA) occurred mainly at the edge sites.[19]

However, despite that the experimental studies listed above showed strong evidence of the influence of the catalyst structure (hence, of the local topology characterizing the reacting surface sites) on the catalytic behavior they lack atomistic level information, which made it possible to only infer on the reasons behind the observed structure sensitivity. Therefore, a theoretical analysis of the structure sensitive phenomena involved in the title reaction may conversely provide new insights into the relationship between shape and size of the catalytic particles and their activity and selectivity.[20]

In fact, catalytic processes, including methanation on different Ni facets, characterized by peculiar steps, kinks and terraces,[21] methanol and ethanol oxidation on different planes of several metals[22–24] as well as water-gas-shift reactions occurring on various planes of both Cu and Pt catalysts[25,26] were recently investigated both by quantum mechanical, namely density functional

theory (DFT), and Monte Carlo approaches. The results consistently demonstrated that the activity and selectivity of the considered reactions were structure sensitive, actually proving the essential role of the computational approaches to catch atomistic insights into this distinctive behavior.

Catalytic reactions usually follow Langmuir-Hinshelwood mechanism, which includes as critical step the chemisorption of the reactants on the surface. Structure sensitivity could thus be linked to the competition among the different kinds of bonds (present in the adsorbed species) to be activated. The latter statement may be ascribed to two main issues related to metal catalysts, *i.e.* substrate coordination and surface site topology, characterizing the rate limiting steps. Therefore, a theoretical analysis capable of quantifying such interactions could be decisive in the enlightenment of the driving forces at the roots of structure sensitivity in catalysis. A joint approach involving experimental and theoretical analyses could be hence exploited for rational catalyst design, in order to achieve the highest activity and selectivity.[3]

In the present work, we studied the selective hydrogenation of MBY to MBE by experimental and theoretical tools. In particular, in order to elucidate the relationship between catalyst structural features and sensitivity, the adsorption of MBY and MBE on a Pd_{30} cluster, showing both {100} and {111} faces and low coordination sites, has been extensively analyzed along with the over-hydrogenation pathways of given MBY/Pd and MBE/Pd surface configurations in the frame of DFT paradigms. The results were subsequently validated experimentally by gas-phase and water-assisted-gas-phase hydrogenation of MBY and MBE performed over supported Pd nanoparticles of well-defined shape and size: Namely, Pd cubes of 10 and 18 nm in edge length enclosed by Pd {100} planes and octahedra of 37 nm in edge length enclosed by {111} planes immobilized on commercial SiO_2. Sound agreement between experimental and computational findings was found, showing how the synergistic use of experimental and theoretical tools can lead to pinpointing the atomistic reasons behind the observed structure sensitivity characterizing metal catalyzed reactions.

Materials and methods

Computational details

All the calculations were performed using the Gaussian 09 package.[27] The hybrid Becke's three parameters exchange-correlation functional B3LYP[28–30] was used throughout the calculations. Los Alamos LANL2 effective core potential and the corresponding valence basis set were used for Pd atoms; the corresponding D95 basis sets for O, C and H atoms were added of the LANL2dp polarization functions.[31] The B3LYP/LANL2DZ model chemistry has been chosen because it has been found reliable for systems formed by organic molecules adsorbed on palladium.[32]

The starting Pd_{30} cluster model was obtained cutting a fragment (embodying both {100} and {111} faces) from the Pd *fcc* bulk structure (space group $Fm\bar{3}m$, being $a = 387.9$ pm) and then fully optimizing its geometry (see Figure 1). The choice of this particular cluster allowed us the simultaneous study of all the relevant sites (*i.e.* surface, edge and corner atoms present on different planes) in a single model. In this way, we avoided to mimic the sites of interest by using differently shaped and/or sized catalyst models, which would likely bias the inspected properties. As a matter of fact, while the investigation of the surface sites could have been made by periodic calculations, the corresponding simulation of edge and corner sites would have required prohibitively large supercells.

[Figure 1 about here.]

The formation of hydride and/or carbide phases was not considered in the present study: This choice was supported by the modeled experimental conditions, which involved *i*) high temperature (see notes *b* and *c* in Table 3) capable of decomposing metal hydride derivatives[33,34] and *ii*) a relatively long chain-length of the reacting molecules, which was found to significantly reduce the amount of carbide species formation.[35] With respect to this, it is here to be recalled that the atomistic modeling of catalytic systems is necessarily ruled by a compromise between the required accuracy and the corresponding complexity introduced in the adopted models.[36]

In particular, it has here to be emphasized that the present work has been specifically focused on the role of the different palladium sites in ruling the cluster activity, regarding the title reaction. In spite of that, special support functions could be generally involved, as recently restated, when supported catalysts are employed.[37,38] However, such a large-scale effort study is outside of the scope of the here suggested modeling approach.

The representation here employed is, in fact, affected by some approximations but, in our opinion, comprises all the critical aspects characterizing the investigated phenomena. In particular, the resulting inferences, based on the title modeling, refer to experimental results interpreted in terms of energy differences[19] that are well reproduced by the systematic trends found employing the DFT approaches here suggested. All the possible binding sites and adsorption coordinations were indeed tested as starting models for the MBY/Pd_{30} and MBE/Pd_{30} systems. For these, the interaction energies were computed as $\Delta E = E_{sub/Pd_{30}} - (E_{Pd_{30}} + E_{sub})$, being *sub* the adsorbed substrate, *i.e. sub* = MBY, MBE, MBA. Therefore, negative values correspond to the formation of stable aggregates.

On the stablest and unstablest surface configurations of both the MBY/Pd_{30} and MBE/Pd_{30} systems, whole hydrogenation energetics were also evaluated. The transition states (TSs) involved either in the MBY to MBE or in the MBE to MBA hydrogenation were located using the Berny algorithm and their properties were characterized by inspection of the normal mode associated with the corresponding imaginary harmonic vibrational frequencies. All the energy values reported in the present work were corrected for the zero-point vibrational contribution. BSSE can not affect the conclusions of the present study, since the former are based on differential analyses of adsorption energies characterized by very large values, which are involved in systems that each other differ only for the surface placements of the considered molecules on the same palladium cluster.

Experimental details

Catalyst preparation

Pd nanocubes of 10 and 18 nm of edge length and octahedra of 31 nm of edge length were prepared, following protocols published elsewhere.[39–41] In order to prevent agglomeration, polyvinyl-pyrrolidone (PVP) was used as stabilizing agent in all cases. The final products were collected by centrifugation and washed with an ethanol/water solution to remove excess PVP. The as prepared nanoparticles were then immobilized on commercially SiO_2 (S5505 Sigma-Aldrich) by wet impregnation.

Catalyst characterization

To determine the amount of Pd in each sample, the supported catalysts were analyzed by atomic absorption spectroscopy (AAS) using a Shimadzu AA-6650 spectrometer. The specific wavelength used for Pd^{2+} was 475 nm. Shape and size of the unsupported as well as of the supported nanoparticles were analyzed by transmission electron microscopy (TEM), using a Philips CM20 microscope operated at 200 kV.

Active metal dispersion and surface area were determined through CO chemisorption using Autochem II 2920 (Micromeritics). The samples were loaded into a U-shaped Quartz cell (3.76 mm i.d.), heated in 20 cm^3 min^{-1}, under a 2% H_2/He mixture, at 10 K min^{-1} to 373 K and subsequently held at that temperature for 15 min. The samples were then out-gassed in Ar at 373 K for 30 min and finally temperature was decreased to ambient conditions. The CO-chemisorption experiments were performed at 323 K using He as carrier gas. A 3% CO/He mixture was pulsed through the sample until the peaks were equal. In a series of blank tests, chemisorption measurements on SiO_2 did not result in any detectable CO uptake.

Catalytic testing

MBY hydrogenation was carried out in vapor-phase at atmospheric pressure in a fixed bed differential tubular reactor. A layer of borosilicate glass beads served as a preheating zone, ensuring that the reactant was vaporized and reached reaction temperature before contacting the catalyst. The reaction temperature was continuously monitored by a thermocouple inserted in a thermowell within the catalyst bed. The reactant was delivered to the reactor *via* a glass/teflon airtight syringe and teflon line using a microprocessor controlled infusion pump (Model 100 kd Scientific) at a fixed flow rate and hydrogen and argon were fed co-currently. The reactor effluent was condensed in an ice cold water trap for subsequent analysis, which was made using a Perkin-Elmer Auto System XL gas chromatograph equipped with a programmed split/splitless injector and a flame ionization detector, employing a 30 m Stabilwax (Cross-Bond Carbowax-PEG, Restek, USA) 0.32 mm capillary column with a 0.25 μm coating.

Results and discussion

DFT results

MBY and MBE adsorption modes on Pd surfaces

As we already observed in the MBY liquid-phase hydrogenation,[19] the catalytic performance of Pd is closely related to the involved adsorption sites, *i.e.* it is a structure sensitive reaction. In fact, the triple to double bond reduction seemed to occur four times faster on plane than on edge or corner sites. Conversely, the full saturation of the olefin seemed to occur almost exclusively on the Pd nanoparticle edge sites.

In order to understand the origin of the observed effects, a DFT study on the adsorption modes and hydrogenation reactivity of MBE and MBY on palladium was undertaken on the Pd_{30} cluster – embodying both {100} and {111} faces – described in the Computational Details section. All the possible MBY and MBE adsorption configurations on the cluster sites, present both in the {100}

and {111} faces, were initially investigated. Figure 2 and Figure 3 gather the optimized geometries characterizing the MBY/Pd_{30} and MBE/Pd_{30} adsorption systems, respectively. The corresponding acronyms individuate the hapcity (η) and the bridging ability (μ) of the ligands (MBY, MBE) along with the topological properties of the involved surface sites: P, E, C categorize plane, edge and corner interacting sites while the subscript pairs 00, 11 and 10 emphasize if the same sites belong to the faces {100}, {111} or to both. When specific naming for the adsorption modes is not necessary, the generic P, E, C labels without further specifications are employed.

[Figure 2 about here.]

[Figure 3 about here.]

Figure 4 shows the adsorption energies characterizing different MBY and MBE species over Pd_{30} systems *versus* the corresponding carbon-carbon bond (C≡C, C=C) distances. Clearly, the increase of the interaction energy values with the carbon-carbon bond elongation are fairly more pronounced for the MBY systems and, in all cases, the interaction energies are higher than those of the MBE systems.[§]

[Figure 4 about here.]

An MBY molecule singly adsorbed by the C≡C bond on the plane sites, of both the {100} and {111} faces, corresponding to the (μ_2:μ_2-MBY)P_{00} and (μ_2:μ_2-MBY)P_{11} systems of Figure 2, interacts by 2 bridge coordinations with four and three Pd atoms of the cluster, respectively. Moreover, significantly large carbon-carbon bond distances (*ca.* 142 and 137 pm) are observed for these configurations, leading to elongations (referred to the isolated MBY molecule) of about 17 and 13%.

On the other hand, on corner and edge sites the MBY surface species interact with just one Pd atom, except for the (μ_2-MBY)E_{10} and (μ_2-MBY)E_{11} adsorption modes that show one single bridge interaction, involving two surface sites. The latter configurations are characterized by an

[§]In passing, it is here recalled that the calculated C≡C and C=C bond distances for the MBY and MBE isolated species resulted 121.5 and 134.0 pm, respectively

elongation of *ca.* 9% while the remaining ones, namely those in which MBY interacts with only one Pd site, of *ca.* 5%. Interestingly, carbon-carbon distance elongations increase when the interactions involving the MBY surface derivatives encompass bridging adsorptions, which also seem more probable to occur on plane rather than on corner/edge sites.

A different behavior is observed for the MBE derivatives: Bridge adsorption, associated with a sensible carbon-carbon bond elongation (*ca.* 10 pm) was found only in the (μ_2-MBE)P_{00} case while the other MBE interactions with the remaining surface sites, either of {100} or {111} faces, occurred exclusively in the η^2 configuration. Accordingly, small carbon-carbon bond lengthening (*ca.* 4%) were calculated. For the MBE systems, the interaction energies resulted in any case less marked than those observed for the MBY ones, being the weakest that of the only bridged derivative occurring on the {100} face, namely the (μ_2-MBE)P_{00} plane configuration above (see Figure 4).

This occurrence is not surprising since the MBE carbon atoms of the C=C μ_2 moiety, which interact with the metallic surface have a larger sp^3 character than those of the η^2 one. Therefore, the μ_2 carbon atoms should be locally affected by a larger steric hindrance especially if the surface interactions occur on the plane instead of corner/edge sites. Figure 4, finally, outlines that the bond elongations and interaction energies are on average lower for the MBE with respect to the MBY surface derivatives while relating the MBY and MBE adsorption energies to the activation of their unsaturated carbon-carbon bonds and the activation to the reactivity, three main points arise:

- Irrespective of the {100} and {111} palladium faces, the C≡C moiety, characterizing the interacting MBY surface species, should be activated preferentially by plane sites.

- On the other hand, MBE species have to adsorb either on corner or edge sites to give rise to large adsorption energies, hence to the strong surface interactions necessary for the activation of the C=C moiety.

- From a general perspective, MBY should be more reactive than MBE, when hydrogenated on palladium.

The first two points seem to confirm the hypotheses already formulated for the liquid-phase hydrogenation of MBY and concerning the dependence of the found activity on the characteristic adsorption energies of MBY and MBE on the different sites of Pd nanoparticles.[19] However, the interaction energy values discussed above not only confirm a higher hydrogenation rate of MBY on plane sites – whereas MBE hydrogenation should occur mainly on low coordination, namely edge or corner, sites – but also predict a higher absolute value of activity for MBY as compared to MBE (see third point). This result is not obvious since the general behaviour of alkynes and alkenes in gas phase or in solution is not necessarily the same when the unsaturated bonds are framed in molecules with different substituents, especially if adsorbed on metallic surfaces.

Mechanistic studies

With the aim to further validate the findings of the preceding section, investigations on the MBY and MBE hydrogenation over the Pd_{30} cluster were performed in order to verify whether the involved energy barries could also play a role in the structure sensitivity of the reaction in unison with the thermodynamic-drive found in the previous section. The ensembles of binding modes considered representative of the adsorption processes for both MBY and MBE on the Pd_{30} cluster are each composed by eight configurations (see Figure 2 and Figure 3), occurring on topologically non-equivalent metallic sites. Within this ensembles two binding modes for the MBE and two for the MBY were selected as starting point. The choice was carried out considering the two limit variations of the carbon-carbon unsaturated bond caused by the interaction with the metallic cluster, *i.e.* those two configurations where the largest and the smallest elongation of the carbon-carbon unsaturated bond is found, were selected. It is, in addition, assumed throughout that atomic hydrogen is available on the Pd_{30}, since relatively low energy barriers have been calculated for H_2 fragmentation and H diffusion on palladium clusters.[42]

MBY to MBE Hydrogenation Among the eight possible MBY configurations on the Pd_{30} cluster, the (μ_2:μ_2-MBY)P_{00} and (η^2-MBY)C_{11} ones were selected for evaluating the hydrogen co-

adsorption processes. The first configuration shows the MBY molecule adsorbed on the {100} plane and each carbon atom of the C≡C moiety bridges 2 Pd atoms. According to our calculations, in this configuration the oxygen atom of MBY does not interact with the surface sites because of the increase of torsional strain that the molecule would have to undergo with that additional interaction. Conversely, in the (η^2-MBY)C_{11} configuration, MBY undergoes a double interaction with the cluster through both the C≡C moiety and the oxygen of the alcoholic group. The triple bond is indeed coordinated to a single corner palladium atom while the alcoholic oxygen is adsorbed on a Pd atom, belonging to the edge of the cluster (corner/edge arrangement). The (μ_2:μ_2-MBY)P_{00} configuration with co-adsorbed hydrogen was found to be more stable than the (η^2-MBY)C_{11}, being the energy difference *ca.* 86.3 kJ mol^{-1}. For both these co-adsorbed systems, two possible hydrogenation mechanisms were considered, involving Markovnikov-like and *anti*-Markovnikov-like addition of hydrogen to the activated triple bond.[¶]

[Table 1 about here.]

The first step of both mechanisms imply the addition of the chemisorbed hydrogen to the MBY triple bond, thus producing a partial hydrogenated intermediate, which, in a second step, is subsequently hydrogenated to MBE. Irrespective of the topological configuration, as summarized by Table 1, the Markovnikov hydrogen addition shows, on the whole, a lower energy barrier (E_b) value for the rate determining step (*i.e.* for the step showing the highest E_b value). The Markovnikov mechanism was therefore considered to be the most likely. Comparing the (μ_2:μ_2-MBY)P_{00} and (η^2-MBY)C_{11} surface configurations, it is interesting to note that the carbon-carbon distance parameter changes in a significant way, in these systems, on the contrary the same parameter remains almost unaltered when considered for the same configuration, undergoing Markovnikov or *anti*-Markovnikov pathway. This is in agreement with the energy barriers trends that are very similar and can be explained because the different intermediates are stabilized in a similar way by the catalyst. Thus, the only feature discriminating among the hydrogenation pathways is the initial

[¶]The names of these mechanisms are given in analogy to those characterizing halogenidric additions to C=C moieties; from now on, for sake of simplicity we will refer to them as Markovnikov and *anti*-Markovnikov mechanisms.

topological MBY configuration, as shown in Figure 5. In fact, comparing the Markovnikov reaction mechanisms of the two considered configurations, clearly results that the slightly favored energetics characterizing the (η^2-MBY)C_{11} configuration are not enough to overcome the starting energy difference between the two binding modes that evidently favor the (μ_2:μ_2-MBY)P_{00} configuration.

[Figure 5 about here.]

MBE to MBA hydrogenation The (η^2-MBE)C_{00} and (η^2-MBE)P_{11} topological configurations were selected to study the second hydrogenation step, *i.e.* the MBE $\longrightarrow$ MBA process on the Pd_{30} cluster, hypothesizing Markovnikov and *anti*-Markovnikov mechanisms. The choice of the configurations above, as for those of the MBY systems of the preceding section, was ruled by the smallest and the largest carbon-carbon bond elongations involved in the C=C moiety (see Figure 4), following the MBE surface site interactions. In this regard, it has to be underlined that the (μ_2-MBE)P_{00} derivative was here not considered because, as already explained, due to the hindered surface interactions of the adsorbed MBE, it is out of line with respect of the remaining topological configurations.

In the (η^2-MBE)C_{00} configuration, the MBE C=C moiety is coordinated to a corner Pd site while the alcoholic oxygen, as in the case of the (η^2-MBY)C_{11} configuration, interacts with a Pd site, belonging to the edge of the metallic cluster (corner/edge arrangement). On the other hand, in the (η^2-MBE)P_{11} configuration MBE is bonded to one {111} plane site of the Pd_{30} cluster and shows a further interaction *via* the alcoholic oxygen to an edge site of the same cluster. Considering the co-adsorbed H_2 systems, the (η^2-MBE)C_{00} configuration was found to be more stable than the (η^2-MBE)P_{11} one with a difference in energy of 73.0 kJ mol^{-1}. Interestingly, the energy difference between the two initial MBE configurations is less pronounced than that of the MBY configurations.

As in the case of the MBY hydrogenation, the energy barriers for the Markovnikov and *anti*-Markovnikov mechanisms, regarding the same topological configuration, are not very different

(see Table 1). This finding agrees with the observed correspondence occurring among the carbon-carbon distances, characterizing all the different MBE adsorbed systems (see Figure 4). Nevertheless, it was found that the Markovnikov mechanism is favored, irrespective of the initial MBE configuration. The corresponding hydrogenation trends are illustrated in Figure 6, both for the (η^2-MBE)C_{00} and (η^2-MBE)P_{11} co-adsorbed H_2 systems.

[Figure 6 about here.]

The reaction paths for these configurations are similar, showing a larger E_b value in the first half-hydrogenation step and follow the same trend found for the hydrogenation of *cis*-but-2-ene to *n*-butane on a small Pd cluster.[43] Also in this case, as already observed for both the MBY half-hydrogenation steps, the differences in the calculated E_b values are, however, not influential in setting the preferred reaction mechanism. Conversely, the latter is, once more, controlled by the difference in the adsorption energies between the two binding modes, clearly favoring the corner/edge (η^2-MBE)C_{00} system. This result agrees with the experimental evidences that led Crespo-Quesada et al. to claim that the low coordination sites are preferred in the MBE to MBA hydrogenation on palladium crystallite.[19]

Therefore, the *in vacuo* DFT calculations are able to capture all the principal features of the over-hydrogenation of MBY on well-defined size- and shape-controlled palladium nanoparticles, in particular shedding light on the origin of its structure sensitivity, observed in liquid-phase.[19] Moreover, looking at Figure 4 and Table 1 it is possible to infer that Pd catalysts, mostly showing both {100} and {111} faces,[20] should be very selective in respect of the first half-hydrogenation of MBY. This is attributable to two main factors:

- The higher surface interaction energies, which on the average favor the adsorption of MBY with respect of MBE over Pd sites.

- The smaller E_b values of both the single steps involved in the Markovnikov mechanism – that was demonstrated to be always more probable than the *anti*-Markovnikov one – of MBY with respect to those of MBE half-hydrogenations.

Experimental results

Four palladium catalyzed MBY to MBE hydrogenation routes were investigated by DFT and, as reported by Crespo-Quesada et al., it was found that corner/edge sites are less active if compared to plane sites, being the primal cause of this phenomenon linked to the MBY adsorption energies, which change with the adsorption sites, and not to the energy barriers involved in the surface reaction steps.[19] Moreover, if the adsorption energy values are accepted as a descriptor of the carbon-carbon bond activation of the interacting species, hence of their reactivity, we could infer from Figure 4 that MBY and MBE should be preferably hydrogenated on {100} and {111} planes, respectively. In order to check the latter statement, not yet experimentally investigated, a new set of experiments in bi-phase conditions was undertaken, also deepening the role of the water molecules in the same catalytic reactions.

Catalyst preparation and characterization

We prepared Pd nanocubes of 10 and 18 nm of edge length (CUB_A and CUB_B) and octahedra of 31 nm of edge length (OCT).[39–41] After being thoroughly washed to remove excess PVP, the nanoparticles were immobilized on SiO_2 by wet impregnation leading to a weight percent of supported palladium ($wt_{\%Pd}$) equal to 1.8, 5.0 and 3.6, for CUB_A, CUB_B and OCT, as determined by atomic absorption spectroscopy. Figure 7 sets out TEM micrographs of the freshly supported nanoparticles, showing shape stability after deposition. TEM images of the unsupported (as prepared) nanoparticles, along with their detailed morphological characterization can be found elsewhere.[19]

[Figure 7 about here.]

Table 2 summarizes the main properties of the catalysts: Palladium weight percent, edge-length of the metal nanocrystallites (d_{nc}), expected and experimental metal dispersion (D_{expc} and D_{expm}) and metallic surface area (A^{M}_{expm}). It can be observed that the D_{expm} values were lower than those expected, D_{expc}, for the corresponding *fcc* Pd crystallites, considering once face to be unavailable for chemisorption due to the interaction with the support.[44] The difference was highest

for the most concentrated catalysts, as it could be expected when immobilizing nanoparticles by wet impregnation. However, this allows one to independently observe either size effects, through the comparison of CUB_A and CUB_B behaviors while keeping the same crystallographic plane exposed, or shape effects, through the comparison of CUB_B and OCT activities while keeping the dispersion constant.

[Table 2 about here.]

MBY hydrogenation in the gas-phase

We tested the aforementioned catalysts in the gas-phase hydrogenation of MBY and MBE. The equivalent size for isolated Pd nanoparticles corresponds to the range of 15-50 nm and, therefore, edge and corner effects are negligible as compared to planar effects. The following results aim at validating the results obtained by DFT calculations with respect to the relative reactivity of Pd {100} and {111} planes in the hydrogenation of alkynes and alkenes, respectively.

We performed the catalytic experiments in a differential tubular reactor. In such reactors, the thickness (1-2 mm) of the catalytic bed as well as the conversion (*ca.* 15%) are low enough to guarantee gradient-less operations, *i.e.* the reaction rate is constant in all the points of the bed. In this case the plug-flow performance equation can be written as:

$$\frac{m_{cat}}{F_{i,in}} = \int_0^X \frac{dX_i}{-R_i} = \frac{1}{-R_i}\int_0^X dX_i = \frac{X}{-R_i} \tag{1}$$

the transformation rate, $-R_i$, can be, therefore, calculated as:

$$-R_i = \frac{C_{i,in} - C_{i,out}}{\frac{m_{cat}}{Q_T}} \tag{2}$$

where F_i is the molar flow-rate of i, m_{cat} the mass of catalyst in the reactor, X_i and X the i^{th} species conversion and the whole conversion, respectively, C_i the concentration of i and Q_T the total volumetric flow-rate. TOF can be then calculated, using a given expression of the metal

dispersion (D), see Table 2:

$$\mathrm{TOF} = -\mathrm{R_i D} \tag{3}$$

Since relatively large particles were used in this study, the dispersion can be directly correlated with planar atoms, hence the obtained TOF can be considered to arise exclusively from Pd {111} or {100}, for OCT or CUB samples, respectively. Figure 8 shows the observed activity, as TOF, for the three catalysts in the hydrogenation of MBY (grey bars) and MBE (black bars).

The first observation that can be made is that the reactivity of the Pd/SiO_2 catalysts was highest in the hydrogenation of MBY over Pd {100} plane which is in line to the computational results that showed the strongest interaction energy for this pair (-205 kJ mol^{-1}), hence a considerable increase in bond length from 121.5 pm, for isolated, to 142.5 pm for adsorbed MBY.

[Figure 8 about here.]

With respect to MBY hydrogenation, the experimental results are consistent with the DFT calculations, showing that the activity of the Pd {100} planes were approximately four times higher than for the Pd {111}. Although MBY hydrogenation is known to be a structure sensitive reaction,[19] the activity for both CUB_A and CUB_B was found to be the same within the experimental error, which could be expected since corner and edge effects are negligible for nanoparticles larger than 15 nm. Selectivity towards MBE (*i.e.* S_{MBE}), on the other hand, did not seem to be affected by the crystallographic plane, being consistently 84.7 ± 1.5 %, regardless the involved planes . The evidence that both planes produce MBE with the same specificity may be ascribed to the fact that the mode of adsorption of MBY is very similar on both Pd {111} and {100} planes, as shown by the two most stable topological configurations found by DFT calculations: (μ_2:μ_2-MBY)P_{00} and (μ_2:μ_2-MBY)P_{11}. Different adsorption modes have indeed been usually related to the formation of different reaction intermediates, and thus, products.[45,46] Since both planes seem to interact with MBY in the same manner, the same reaction intermediate leading to MBE is presumably formed. This value of selectivity is significantly lower than the one found in our previous study with unsupported Pd nanocrystals in the liquid-phase hydrogenation of MBY.[19] This could be attributed to the

difference in the H_2 : MBY molar ratio which varied from 1.5 : 1 in the gas-phase to approximately 1 : 25 in the liquid-phase.

Regarding MBE hydrogenation, there is also concurrence between experimental and computational findings. In fact, while DFT calculations predicted a higher activity for Pd {111} as compared to {100} planes due to a more activated adsorption mode for the former, experimental results showed precisely the same trend. The activity found for {100} planes was $5 \pm 1 s^{-1}$, whereas for {111} it was $13 \pm 2 s^{-1}$. It is worth noting that MBE hydrogenation presented lower TOFs as compared to MBY, which is in agreement with the smaller bond distortion (see Figure 4) and with the pairs of E_b values, singly involved in the Markovnikov MBY and MBE half-hydrogenation, calculated for the latter and illustrated in Figure 5 and Figure 6.

As mentioned before, conversion was kept purposely low in order to ensure differential reaction conditions. However, based on the above results, it could be expected the kinetics of each plane to be significantly different, especially at high conversions. Whereas Pd {100} planes should remain relatively selective towards MBE up to high conversions based on its low activity towards MBE, {111} planes should, on the other hand, present a significantly lower selectivity at high conversions since TOF_{MBE}:TOF_{MBY} was found to be approximately 0.33. Some hints to explain this result can be again extracted from Figure 4. In fact, the stability order of the plane species follows the sequence: (μ_2:μ_2-MBY)P_{00} > (μ_2:μ_2-MBY)P_{11} > (η^2-MBE)P_{11} > (μ_2-MBE)P_{00}. Furthermore, the adsorption energy difference between MBY and MBE on {100} and {111} planes is about double in the first with respect of the second plane. Considering this and the fact that the MBE {100} plane species is the only one characterized by an interaction energy falling within the physisorption value range, it can be inferred that: Unlike the {111} plane where the MBE – just formed on the Pd surface by the first MBY half-hydrogenation – could compete with the not yet adsorbed MBY, in the {100} plane we should observe a very low, if any, competition between MBY and MBE hydrogenation.

MBY hydrogenation in the gas-phase: The effect of water

The conditions used in the aqueous over-hydrogenation of MBY on well-defined size- and shape-tailored palladium nanoparticles[19] were, as already mentioned, somewhat more distanced from DFT than in the gas-phase with pure reactants. Indeed, there are a few discrepancies between the liquid-phase results and the ones presented here. Namely, in the liquid-phase study, Pd {111} and {100} planes were found to be roughly equally active towards the hydrogenation of MBY while {111} planes were not found to be very active with respect to MBE hydrogenation. Therefore, gas-phase MBY and MBE hydrogenations in the presence of water were also carried out here to elucidate if the divergent results between liquid- and gas-phase studies could arise due to solvent effects.

Table 3 shows the findings obtained using a 50/50 v/v mixture of MBY and water as feed. From the results reported in Table 3 and recalling those summarized in Figure 8, it can be observed that *i*) water indeed influences the reactivity towards MBY hydrogenation and *ii*) both planes are roughly equally active and behave quite similarly to the liquid-phase. It is possible to compare activities even at different concentrations, since MBY hydrogenation has been reported to be of zero order with respect to the alkyne in both solvent-free[47] and water-assisted[19] conditions. Interestingly, water was found to exert an effect on the Pd {100} but not on the {111} plane. Concerning selectivity, water did not seem to have a relevant effect, suggesting that the mode of adsorption of MBY remains unaltered also in the presence of water.

[Table 3 about here.]

Since in the liquid-phase study it was found that planar atoms were almost inactive in the hydrogenation of MBE, we repeated the aforementioned experiment using MBE in the feed, too. Due to the immiscibility of the MBE/water mixture, a solution 5/95 v/v was used in this case. As it can be noticed from a look to Table 3, the values continue to follow the trends observed with pure MBE but the transformation rates obtained are much lower. Moreover, the order of the reaction is, in this case, complex and it is therefore difficult to compare both results. In fact, in

the liquid-phase reaction, the molar H_2O : MBE ratio was 1000 and the maximum concentration of MBE was 40-60 mol m^{-3} while the activity of the planes remained negligible. On the other hand, the concentrations in the gas-phase ranged from 1 mol m^{-3} in solvent-free conditions to 0.04 mol m^{-3} in the water-assisted experiments and the H_2O : MBE ratios ranged from 0 to 100, respectively. The fact that higher MBE concentrations with higher H_2O : MBE ratios (liquid-phase conditions) led to lower reaction rates than in the gas-phase suggests that water does actually exert an influence on planar reactivity. Possible explanations include surface regeneration (cleaning) or co-adsorption of water, with a heat of adsorption intermediate to that of MBY and MBE.

The role of the H_2O molecules, as explained above, would seem primarily related to the competition for surface sites. In any case, this competition would induce cleaning/renewing of the vied sites. As a consequence, the selectivity could increase as the water molecule content increases in the reaction environment (liquid-phase $>$ water-assisted-gas-phase $>$ gas-phase), since the competition is maximally exerted on the less strongly adsorbed species, namely the MBE surface derivatives.

Conclusions

The DFT results were found to be consistent with the experimentally observed trends characterizing the structure sensitive over-hydrogenation of MBY on well-defined size and shape-controlled Pd nanocrystallites. The calculated adsorption energies characterizing the interactions of MBY and MBE with palladium sites, which originate from different surface topologies, could be related to both activity and selectivity experimental trends. The synergistic use of experimental and theoretical tools allowed us to describe the structure sensitivity effects observed in the semi-hydrogenation of MBY to MBE and MBE to MBA over well-defined size and shape-controlled Pd nanocrystallites, thus explaining their observed activity and selectivity.

The DFT energetic description confirms that Pd catalysts, showing both {100} and {111} planes, should be characterized by a very high selectivity to MBE when MBY hydrogenation

occurs. In particular, the C≡C moiety, characterizing the interacting MBY surface species, seem to be activated, by strong interaction energies, preferentially by plane sites with respect to corner/edge atoms. A different behavior is observed for the MBE species. These, to give rise to strong surface interactions activating the C=C moiety, have to adsorb mostly on low coordination (edge/corner) sites. Furthermore, the DFT calculations proves that the considered reaction paths are characterized by similar energy barriers: Plane, edge or corner surface configurations are thus not influential in setting the preferred reaction mechanism, which conversely is controlled by the relative difference in the adsorption energies.

Finally, this study helps to explain the changes – mostly produced by adsorption competition between water molecules and MBY and MBE on the palladium sites – that take place along with the title reaction when this occur in different phases: Gas-, water-assisted-gas- and liquid-phase. By this, the role of the water in the over-hydrogenation of MBY is also unraveled.

Acknowledgement

We thank Prof. Mingshang Jin (Xi'an Jiaotong University, China) for supplying the size- and shape-supported Pd nanoparticles. This work was supported by the POLYCAT project (Modern polymer-based catalysts and micro-flow conditions as key elements of innovations in fine chemical synthesis), funded by the 7th Framework Programme of the European Community; G.A. No. CP-IP 246095 – http://polycat-fp7.eu/.

References

(1) Blaser, H. *Catal. Today* **2000**, *60*, 161–165.

(2) Chen, B.; Dingerdissen, U.; Krauter, J. G. E.; Rotgerink, H. G. J. L.; Möbus, K.; Ostgard, D. J.; Panster, P.; Riermeier, T. H.; Seebald, S.; Tacke, T.; Trauthwein, H. *Appl. Catal., A* **2005**, *280*, 17–46.

(3) Crespo-Quesada, M.; Cárdenas-Lizana, F.; Dessimoz, A.-L.; Kiwi-Minsker, L. *ACS Catal.* **2012**, *2*, 1773–1786.

(4) Boudart, M. *Chem. Rev.* **1995**, *95*, 661–666.

(5) Boudart, M. *Adv. Catal.* **1969**, *20*, 153–166.

(6) Boitiaux, J.; Cosyns, J.; Vasudevan, S. *Appl. Catal.* **1983**, *6*, 41–51.

(7) van Santen, R. A. *Acc. Chem. Res.* **2009**, *42*, 57–66.

(8) Tribolet, P.; Kiwi-Minsker, L. *Catal. Today* **2005**, *105*, 337–343.

(9) Semagina, N.; Renken, A.; Kiwi-Minsker, L. *J. Phys. Chem. C* **2007**, *111*, 13933–13937.

(10) Dominguez-Dominguez, S.; Berenguer-Murcia, A.; Linares-Solano, A.; Cazorla-Amoros, D. *J. Catal.* **2008**, *257*, 87–95.

(11) Semagina, N.; Kiwi-Minsker, L. *Catal. Lett.* **2009**, *127*, 334–338.

(12) Tew, M. W.; Janousch, M.; Huthwelker, T.; van Bokhoven, J. A. *J. Catal.* **2011**, *283*, 45–54.

(13) Semagina, N.; Kiwi-Minsker, L. *Catal. Rev.* **2009**, *51*, 147–217.

(14) Jia, C. J.; Schuth, F. *Phys. Chem. Chem. Phys.* **2011**, *13*, 2457–2487.

(15) Xiong, Y. J.; Xia, Y. N. *Adv. Mater.* **2007**, *19*, 3385–3391.

(16) Xia, Y.; Xiong, Y. J.; Lim, B.; Skrabalak, S. E. *Angew. Chem. Int. Ed.* **2009**, *48*, 60–103.

(17) Telkar, M. M.; Rode, C. V.; Chaudharia, R. V.; Joshib, S. S.; Nalawadeb, A. M. *Appl. Catal., A* **2004**, *273*, 11–19.

(18) Yarulin, A.; Crespo-Quesada, R.; Egorova, E.; Kiwi-Minsker, L. *Kinet. Catal.* **2012**, *53*, 253–261.

(19) Crespo-Quesada, M.; Yarulin, A.; Jin, M.; Xia, Y.; Kiwi-Minsker, L. *J. Am. Chem. Soc.* **2011**, *133*, 12787–12794.

(20) Duca, D.; Varga, Zs.; La Manna, G.; Vidóczy, T. *Theor. Chem. Acc.* **2000**, *104*, 302–311.

(21) Andersson, M. P.; Abild-Pedersen, F.; Remediakis, I. N.; Bligaard, T.; Jones, G.; Engbæk, J.; Lytken, O.; Horch, S.; Nielsen, J. H.; Sehested, J.; Rostrup-Nielsen, J. R.; Nørskov, J. K.; Chorkendorff, I. *J. Catal.* **2008**, *255*, 6–19.

(22) Wang, H.-F.; Liu, Z.-P. *J. Am. Chem. Soc.* **2008**, *130*, 10996–11004.

(23) Ferrin, P.; Mavrikakis, M. *J. Am. Chem. Soc.* **2009**, *131*, 14381–14389.

(24) Wang, E. D.; Xu, J. B.; Zhao, T. S. *J. Phys. Chem. C* **2010**, *114*, 10489–10497.

(25) Wang, G.-C.; Nakamura, J. *J. Phys. Chem. Lett.* **2010**, *1*, 3053–3057.

(26) Stamatakis, M.; Chen, Y.; Vlachos, D. G. *J. Phys. Chem. C* **2011**, *115*, 24750–24762.

(27) Frisch, M. J.; Trucks, G. W.; Schlegel, H. B.; Scuseria, G. E.; Robb, M. A.; Cheeseman, J. R.; Scalmani, G.; Barone, V.; Mennucci, B.; Petersson, G. A.; Nakatsuji, H.; Caricato, M.; Li, X.; Hratchian, H. P.; Izmaylov, A. F.; Bloino, J.; Zheng, G.; Sonnenberg, J. L.; Hada, M.; Ehara, M.; Toyota, K.; Fukuda, R.; Hasegawa, J.; Ishida, M.; Nakajima, T.; Honda, Y.; Kitao, O.; Nakai, H.; Vreven, T.; Montgomery, J. A., Jr.; Peralta, J. E.; Ogliaro, F.; Bearpark, M.; Heyd, J. J.; Brothers, E.; Kudin, K. N.; Staroverov, V. N.; Kobayashi, R.; Normand, J.; Raghavachari, K.; Rendell, A.; Burant, J. C.; Iyengar, S. S.; Tomasi, J.; Cossi, M.; Rega, N.; Millam, J. M.; Klene, M.; Knox, J. E.; Cross, J. B.; Bakken, V.; Adamo, C.; Jaramillo, J.; Gomperts, R.; Stratmann, R. E.; Yazyev, O.; Austin, A. J.; Cammi, R.; Pomelli, C.; Ochterski, J. W.; Martin, R. L.; Morokuma, K.; Zakrzewski, V. G.; Voth, G. A.; Salvador, P.; Dannenberg, J. J.; Dapprich, S.; Daniels, A. D.; Farkas, Ö.; Foresman, J. B.; Ortiz, J. V.; Cioslowski, J.; Fox, D. J. Gaussian 09 Revision C.01. 2009; Gaussian Inc. Wallingford CT 2009.

(28) Becke, A. D. *J. Chem. Phys.* **1993**, *98*, 5648–5652.

(29) Stephens, P. J.; Devlin, J. F.; Chabalowsky, C. F.; Frisch, M. J. *J. Phys. Chem.* **1994**, *98*, 11623–11627.

(30) Lee, C.; Yang, W.; Parr, R. G. *Phys. Rev. B* **1988**, *37*, 785–789.

(31) Check, C. E.; Faust, T. O.; Bailey, J. M.; Wright, B. J.; Gilbert, T. M.; Sunderlin, L. S. *J. Phys. Chem. A* **2001**, *105*, 8111–8116.

(32) Omar, S.; Palomar, J.; Gómez, L. M.; Álvarez-Montero, M. A.; Rodriguez, J. J. *J. Phys. Chem. C* **2011**, *115*, 14180–14192.

(33) Menegazzo, F.; Fantinel, T.; Signoretto, M.; Pinna, F. *Catal. Commun.* **2007**, *8*, 876–879.

(34) Amorim, C.; Keane, M. A. *J. Colloid. Interf. Sci.* **2008**, *322*, 196–208.

(35) Teschner, D.; Révay, Zs.; Borsodi, J.; Hävecker, M.; Knop-Gericke, A.; Schlögl, R.; Milroy, D.; Jackson, S. D.; Torres, D.; Sautet, P. *Angew. Chemie Intern. Ed.* **2008**, *47*, 9274–9278.

(36) Neurock, M. *J. Catal.* **2003**, *216*, 73–88.

(37) Witte, P. T.; Boland, S.; Kirby, F.; van Maanen, R.; Bleeker, B. F.; de Winter, D. A. M.; Post, J. A.; Geus, J. W.; Berben, P. H. *ChemCatChem* **2013**, *5*, 582–587.

(38) Liguori, F.; Barbaro, P. *J. Catal.* **2014**, *311*, 212–220.

(39) Jin, M. S.; Liu, H.; Zhang, H.; Xie, Z.; Liu, J.; Xia, Y. N. *Nano Research* **2011**, *4*, 83–91.

(40) Lim, B.; Jiang, M. J.; Tao, J.; Camargo, P. H. C.; Zhu, Y. M.; Xia, Y. N. *Adv. Functional Mater.* **2009**, *19*, 189–200.

(41) Jin, M. S.; Zhang, H.; Xie, Z. X.; Xia, Y. N. *Energ. Environ. Sci.* **2012**, *5*, 6352–6357.

(42) D'Anna, V.; Duca, D.; Ferrante, F.; La Manna, G. *Phys. Chem. Chem. Phys.* **2009**, *11*, 4077–4083.

(43) D'Anna, V.; Duca, D.; Ferrante, F.; La Manna, G. *Phys. Chem. Chem. Phys.* **2010**, *12*, 1323–1330.

(44) Van Hardeveld, R.; Hartog, F. *Surf. Sci.* **1969**, *15*, 189–230.

(45) Azad, S.; Kaltchev, M.; Stacchiola, D.; Wu, G.; Tysoe, W. T. *J. Phys. Chem. B* **2000**, *104*, 3107–3115.

(46) Andersin, J.; Lopez, N.; Honkala, K. *J. Phys. Chem. C* **2009**, *113*, 8278–8286.

(47) Crespo-Quesada, M.; Grasemann, M.; Semagina, N.; Renken, A.; Kiwi-Minsker, L. *Catal. Today* **2009**, *147*, 247–254.

TOC entry

Structure Sensitivity of 2-methyl-3-butyn-2-ol Hydrogenation on Pd: Computational and Experimental Modeling

Antonio Prestianni, Micaela Crespo-Quesada, Remedios Cortese, Francesco Ferrante, Liubov Kiwi-Minsker, Dario Duca

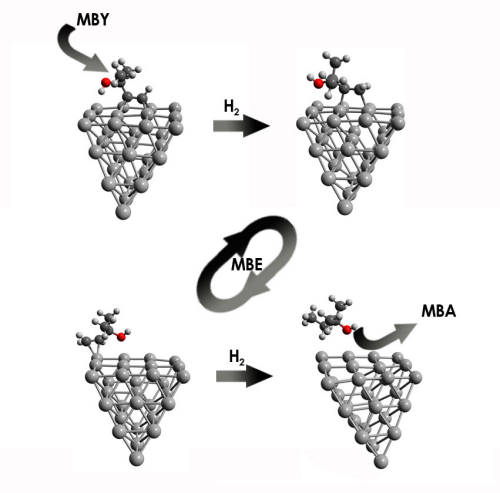

Table 1: Energy barriers, E_b, values of the first and second step involved in the Markovnikov and *anti*-Markovnikov hydrogenation mechanisms for different topological configurations of MBY and MBE species on the Pd_{30} cluster

topological configuration	E_b/kJmol^{-1} [a]	
	Markovnikov	*anti*-Markovnikov
(μ_2:μ_2-MBY)P_{00}	73.0 ǀ 80.5	69.1 ǀ 94.9
(η^2-MBY)C_{11}	79.6 ǀ 49.4	80.2 ǀ 47.6
(η^2-MBE)C_{00}	96.2 ǀ 94.5	97.7 ǀ 87.2
(η^2-MBE)P_{11}	73.2 ǀ 64.1	71.9 ǀ 83.6

[a] The E_b values of the first and the second step of a given hydrogenation, corresponding to the half- and whole-hydrogenation of both MBY $\xrightarrow[H_2]{Pd_{30}}$ MBE and MBE $\xrightarrow[H_2]{Pd_{30}}$ MBA, for a particular surface configuration are reported as pairs separated by a pipe (I step ǀ II step).

Table 2: Catalyst properties: weight percent of palladium, nanocrystallite edge-length, expected and experimental metal dispersion and metal surface area

catalyst	$wt_{\%Pd}$ / %	d_{nc} / nm	D_{expc} / %[a]	D_{expm} / %[b]	A^{M}_{expm} / $m^2\ g^{-1}$ [b]
CUB_A/SiO_2	1.8	10	8.8	7.5	33.5
CUB_B/SiO_2	5.0	18	5.0	2.3	10.4
OCT/SiO_2	3.6	37	3.4	2.8	10.3

[a] Calculated by *fcc* nanocrystal surface statistics,[44] considering one face of the nanoparticles unavailable for chemisorption because of interacting with the support.

[b] Experimentally determined by CO chemisorption.

Table 3: Catalytic MBY and MBE hydrogenation over palladium nanoparticles: Activity, TOF, and selectivity to MBE, S_{MBE}, into water-assisted-gas-phase and liquid-phase conditions

	water-assisted-gas-phase			liquid-phase [a]	
catalyst	TOF_{MBY} / s^{-1} [b]	S_{MBE} / %	TOF_{MBE} / s^{-1} [c]	TOF_{MBY} / s^{-1}	S_{MBE} / % [d]
CUB_A/SiO_2	38.7	87.0	1.2	19.3±2.4	96.0±0.4
OCT/SiO_2	32.3	89.0	1.0	19.3±2.4	96.0±0.4

[a] In the liquid-phase, TOF_{MBE} on the Pd {111} and {100} planes was not evaluated because not very significant, occurring the corresponding hydrogenation just on low coordination sites; on the other hand, Pd {111} and {100} planes behaved similarly in the MBY hydrogenation hence, for the latter, the reported values correspond to both planes. Reaction conditions: $m_{MBY} = 1$ g, $V_{H_2O} = 200$ mL, T = 333 K, $P_{H_2} = 0.3$ MPa, $[MBE]_{max}$ = 50 mol m^{-3}, H_2O : MBE ≈ 1000.[19]

[b] Reaction conditions: MBY : H_2O : H_2 : Ar = 1.5 : 5.5 : 4.5 : 88.5, T = 398 K, P = 1 atm, X≈ 15%.

[c] Reaction conditions: MBE : H_2O : H_2 : Ar = 0.1 : 10.0 : 4.5 : 85.4, T = 398 K, P = 1 atm, X≈15%, $[MBE]_{max}$ = 0.04 mol m^{-3}, H_2O : MBE ≈ 100.

[d] Selectivity at 50% conversion.

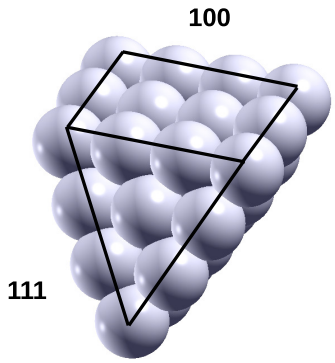

Figure 1: Pd_{30} cluster, showing both {100} and {111} faces.

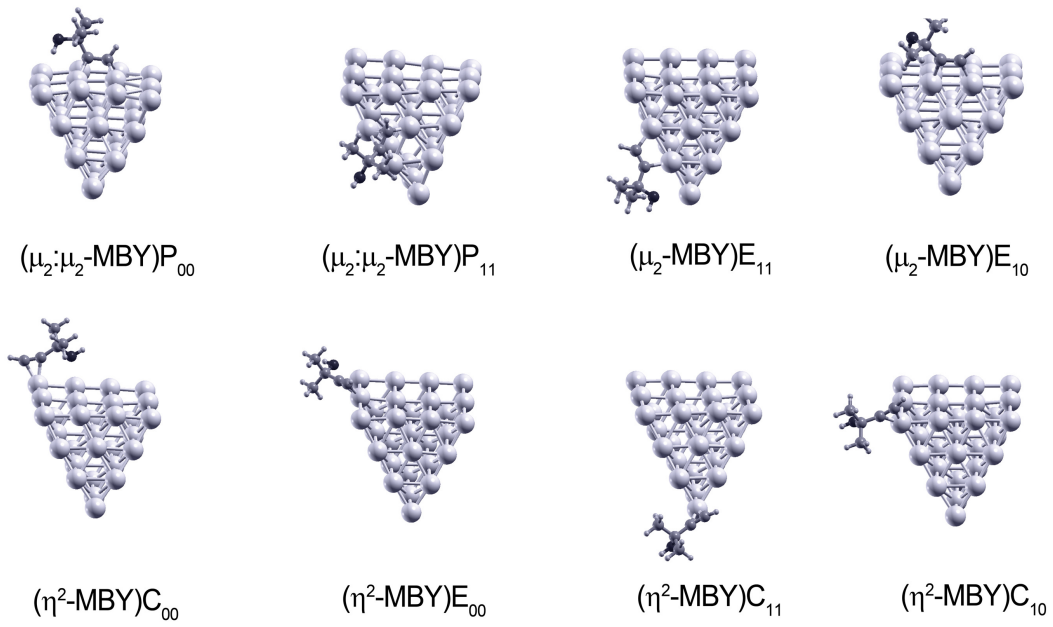

Figure 2: MBY molecule absorbed on different sites of the Pd_{30} cluster; MBY derivative interaction energies decrease from top to bottom and left to right.

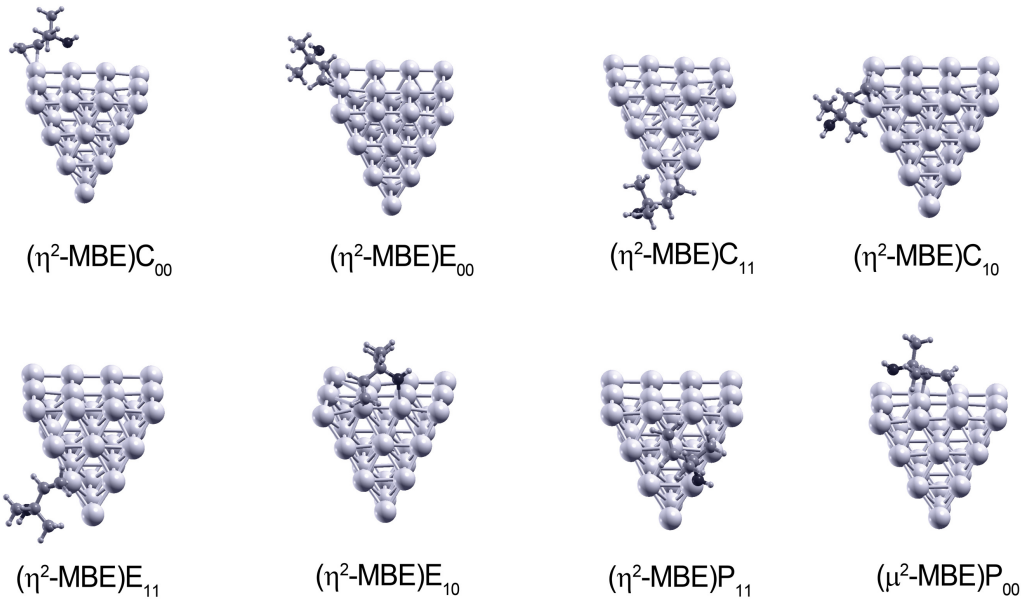

Figure 3: MBE molecule absorbed on different sites of the Pd_{30} cluster; MBE derivative interaction energies decrease from top to bottom and left to right.

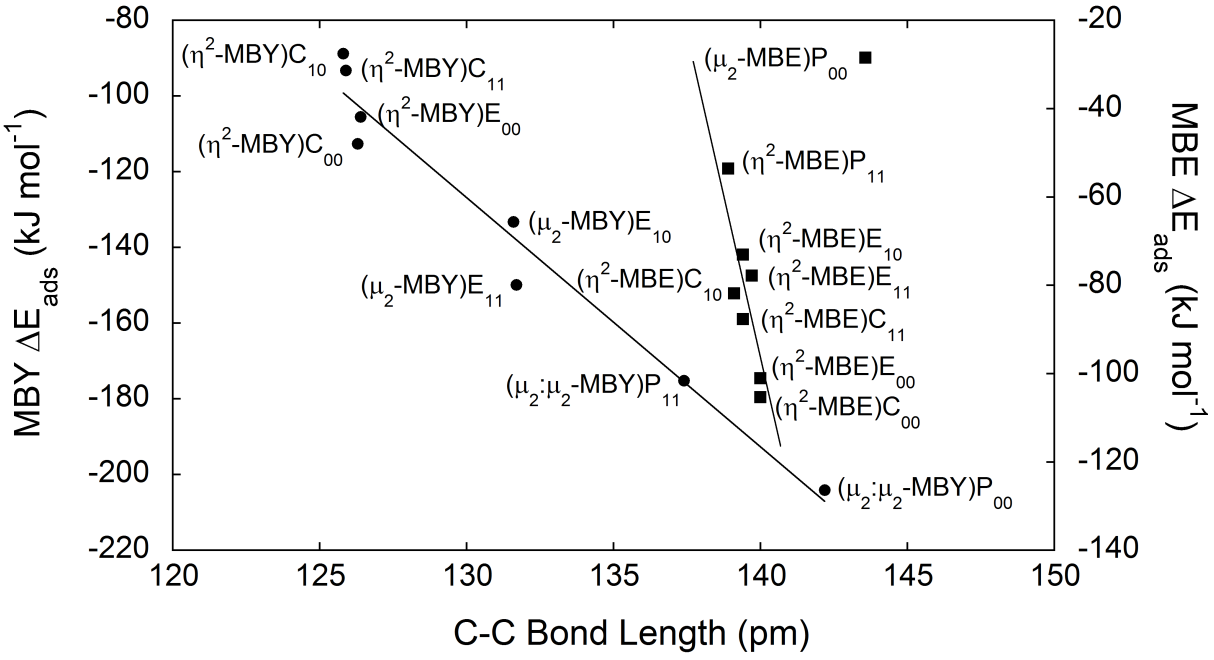

Figure 4: Interaction energies *vs.* carbon-carbon bond distances, characterizing different MBY and MBE adsorption modes over Pd_{30}.

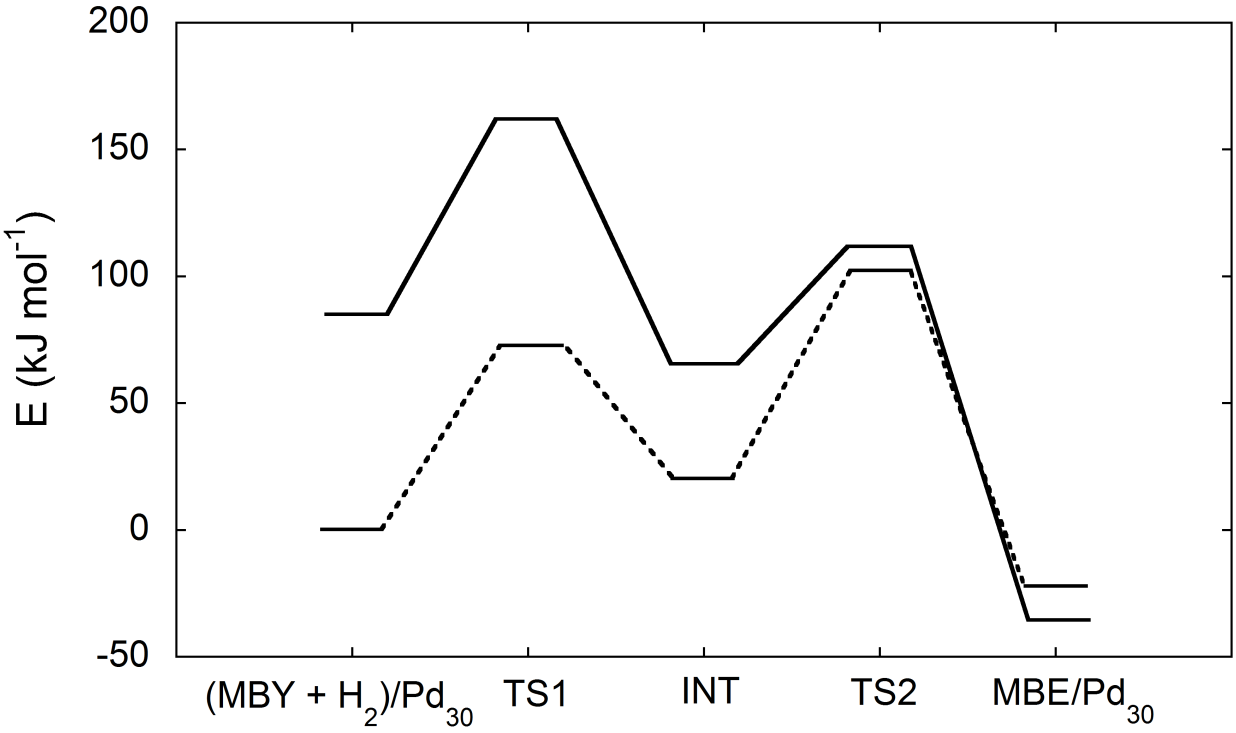

Figure 5: MBY hydrogenation on plane sites, dashed line – starting configuration: (μ_2:μ_2-MBY)P_{00}, and on corner/edge sites, solid line – starting configuration: (η^2-MBY)C_{11}. The MBY + H_2 co-adsorption energy for the (μ_2:μ_2-MBY)P_{00} system is equal to -254.0 kJ mol^{-1}.

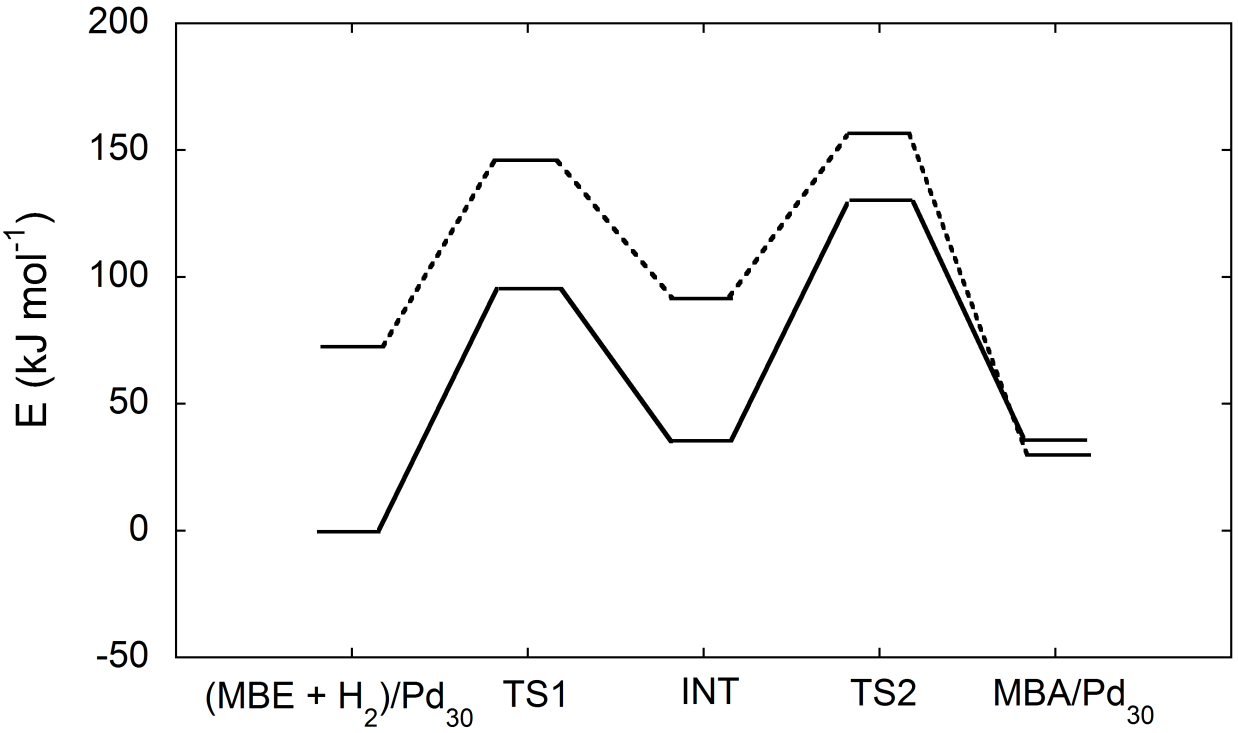

Figure 6: MBE hydrogenation on plane sites, dashed line – starting configuration: (η^2-MBE)P_{11}, and on corner/edge sites, solid line – starting configuration: (η^2-MBE)C_{00}. The MBE + H_2 co-adsorption energy for the (η^2-MBE)C_{00} system is equal to -193.2 kJ mol^{-1}.

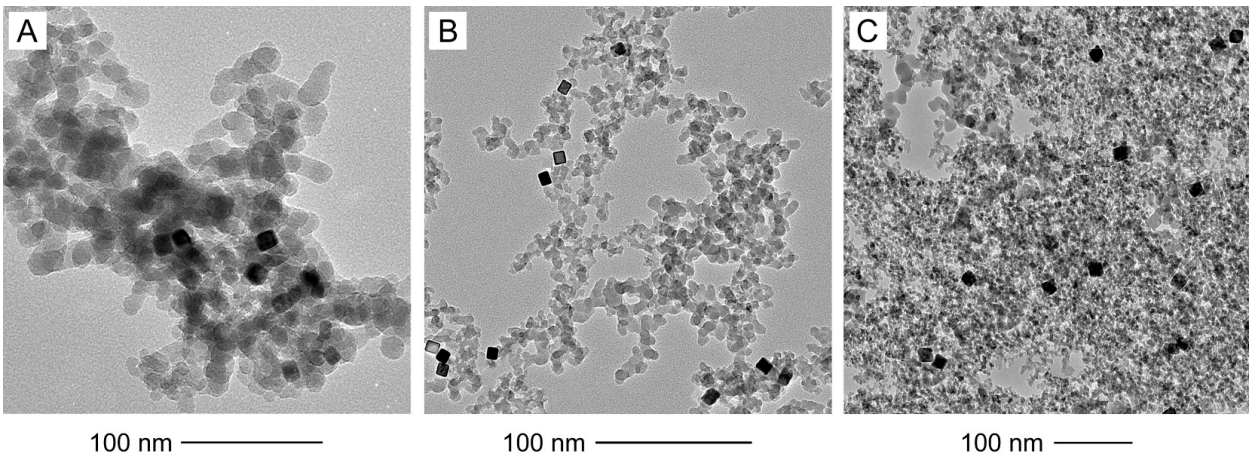

Figure 7: TEM images of the SiO_2-supported A) CUB_A, B) CUB_B and C) OCT Pd nanoparticles.

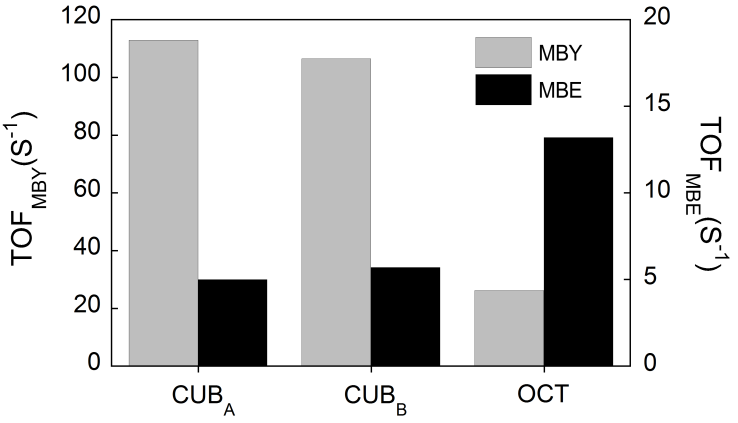

Figure 8: MBY and MBE hydrogenation over CUB_A, CUB_B and OCT catalysts: MBY(MBE) : $H_2 : Ar = 3 : 5 : 92$, T= 398 K, P= 1 atm, X≈15%.